Infragravity Edge Wave Observations on Two California Beaches

JOAN OLTMAN-SHAY* AND R. T. GUZA

Center for Coastal Studies, Scripps Institution of Oceanography, La Jolla, CA 92093

(Manuscript received 23 December 1985, in final form 10 November 1986)

ABSTRACT

Wavenumber–frequency spectra of the infragravity (periods 20–200 sec) wave velocity field in the surf zone of two California beaches are estimated. Because the longshore arrays of biaxial electromagnetic current meters are relatively short (comparable to the wavelengths of interest), high resolution spectrum estimators are required. Model testing provides insight into the limits, capabilities and reliability of the estimators used in this paper. On all 15 days analyzed, between 42% and 88% of the longshore current variance at the array is contributed by low mode ($n \leq 2$) edge waves. (Percentage estimates are not made at a few frequencies because the array is positioned near nodes.) The low mode signal in the cross-shore velocity at the arrays is usually masked by unresolvable high mode and/or leaky waves. The percentage of cross-shore current variance at the array estimated to be low mode is less than 35%, with one exception for which approximately 50% of the variance is mode 0 across a substantial portion of the infragravity band. On average, low mode ($n \leq 2$) edge waves constitute 69% (17%) of the variance of the longshore (cross-shore) infragravity velocities at both arrays. There are days at both beaches that show factors of 3 asymmetry in the energy of up and downcoast progressive edge waves of a particular mode number, but the ratio of up and downcoast energy is usually within 1 ± 0.2. On 8 of the 15 days, the spectrum of swash motions on the beach face is measured with a run-up meter. The swash spectrum, an estimate of the one-dimensional (summed over all wavenumbers) infragravity shoreline elevation spectrum, is compared to the edge wave shoreline elevation variances inferred from the velocity measurements at the array. As much as 50% of the variance in the shoreline swash spectrum is estimated to be contributed by low mode ($n \leq 2$) edge waves. Thus, at least for the present dataset, low mode edge waves contribute significantly to both the longshore velocity and run-up components of the nearshore infragravity wave field. Daily fluctuations in the shoreline elevation variance of individual low mode edge waves are regressed against the total wind and swell wave variance (periods 3–20 sec) measured outside the surf zone. The correlations are statistically significant at one beach, but not the other. Distortions of the observed edge wave dispersion curves (from a plane beach solution) because of beach concavity and mean longshore currents are small but detectable.

1. Introduction

Two alongshore arrays of bidirectional current meters were deployed in the surf zone at Torrey Pines Beach, San Diego and Leadbetter Beach, Santa Barbara. These arrays provided a unique opportunity to estimate the longshore wavenumber–frequency spectrum of motions in the very nearshore with periodic spatial and temporal scales of 20 to 1000 meters and 20 to 200 seconds, respectively. This energy falls just below wind generated surface gravity waves and is commonly referred to as the "infragravity" or "surf beat" frequency band.

Longuet-Higgins and Stewart (1962) suggested a theoretical source of energy for the infragravity frequencies: the second-order forcing, under normally incident wind wave groups, of long waves that reflect at the shoreline and escape out to deep water as free, "leaky" waves. Gallagher (1971) generalized their one-dimensional group forcing model to two dimensions and demonstrated the possibility of resonant second-order nonlinear forcing of edge waves, shallow water surface gravity waves trapped in the nearshore via reflection and refraction. Recently, Symonds et al. (1982) have developed an alternative model for the generation of infragravity energy through the time variation of the breakpoint and the concomitant variation in wave setup. Their model is for a one-dimensional surf zone and therefore cannot generate edge waves but they suggest the "extension to three dimensions is clearly possible."

Munk et al. (1964) were the first to demonstrate clearly the existence of edge waves in the nearshore. They deployed three pressure sensors at a time, in 7 m depth, along a line 500 m offshore and parallel to the coast of Oceanside, California. Over many months their instruments were leap-frogged alongshore until a uniform lagged array (with maximum and minimum lags of 31.4 km and 730 m, respectively) was developed. They calculated (with the assumption of temporal and spatial stationarity) a longshore wavenumber–frequency spectrum and presented some remarkably clear results. In the frequency band of 2 to 12 cycles per hour (cph), they conclusively showed that more than

* Present affiliation: College of Oceanography, Oregon State University, Corvallis, OR 97331.

90% of the energy lay on the dispersion curves of mode 0, 1 or 2 edge waves, the remaining energy falling into the leaky wave continuum. At higher frequencies, 12 to 60 cph, edge wave modes could be recognized but spatial aliasing of the spectrum presented problems.

Munk et al. (1964) demonstrated that edge waves dominate the pressure field 500 meters offshore in 7 meters depth at frequencies of several cycles per hour. However, the relative importance of leaky and edge waves in the very nearshore at infragravity frequencies (roughly 0.3 to 3 cpm) remained unclear. Bowen and Inman (1969, 1971) suggested that longshore periodic features such as beach cusps, crescentic bars and rip currents are formed by standing edge waves. These features, if generated as Bowen and Inman suggest, would require substantial edge wave energy in the surf zone.

Field studies since Munk et al. (1964) have supported the existence of both infragravity leaky and edge waves in the very nearshore. Over the past decade, cross-shore arrays of sensors have been used numerous times to compare the observed cross-shore structure of elevation or velocity with theory. Suhayda (1974) first demonstrated that the cross-shore structure of sea level fluctuations at infragravity frequencies was in good agreement with the theoretical cross-shore standing structure of leaky waves. However, Guza (1974) pointed out that the cross-shore structure of leaky waves and high mode edge waves are almost indistinguishable for the first few zero crossings. To separate edge waves from leaky waves using a cross-shore array, sensors would have to extend considerably beyond the last antinode of the theoretically highest edge wave mode that can be trapped. In addition, the possibility of partial reflection at the shoreline and the possible presence of several modes makes cross-shore arrays generally unsatisfactory for distinguishing edge wave modes and leaky waves (Snodgrass et al., 1962). Therefore, the presence of infragravity edge waves could only be qualitatively suggested from field observations using cross-shore arrays of current meters (Huntley, 1976; Holman et al., 1978; Holman, 1981).

Progressive edge waves were most convincingly demonstrated to exist in the very nearshore from longshore wavenumber–frequency spectra estimated with an alongshore array of bidirectional current meters in the surf zone at Torrey Pines Beach (Huntley et al., 1981). Their two-dimensional spectra showed, for two consecutive days, a lower limit of 30% ± 15% of the variance in the longshore current (0.006–0.023 Hz) to lie either on the mode 0 or 1 edge wave dispersion curves. The cross-shore current indicated dominance by either leaky waves, high mode edge waves or both. On a plane beach of slope β, the infragravity edge wave dispersion relation is discrete (Ursell, 1952),

$$\sigma^2 = gk \sin(2n+1)\beta; \quad n = 0, 1 \cdots \quad \text{and} \quad (2n+1)\beta < \frac{\pi}{2} \qquad (1)$$

where k is the longshore wavenumber, σ is the radial frequency and n the mode number. The complete set of free wave solutions consists of discrete edge waves for $\sigma^2 < gk$ and a continuum of leaky waves for $\sigma^2 > gk$.

The infragravity data of Huntley et al. (1981) presented problems not encountered by Munk et al. (1964). The smaller spatial scale of the infragravity energy made is proportionately more sensitive to tidal fluctuations that changed the array location relative to the shoreline. This restricted data runs to 3 or 4 hours about the high tide mark which in turn reduced the frequency resolution. More serious was the limited wavenumber resolution of the 520 meter longshore array; a 0.015 Hz, mode 1 edge wave has a wavelength of 520 meters. Standard Fourier decomposition of the spatial structure into wavenumber space was therefore inadequate. To increase the wavenumber resolution, Huntley et al. (1981) employed the Maximum Likelihood Estimator (MLE).

A brief description of the two field sites studied in this paper is presented in section 2. Section 3 discusses the high resolution spectrum estimation methods used to obtain satisfactory wavenumber resolution from the relatively short arrays. Appendix A addresses the estimator's limits, capabilities and reliability with synthetic test spectra and the two array configurations. Section 4 presents the longshore wavenumber–frequency spectra observed for both longshore and cross-shore velocities on eight days at Torrey Pines Beach, San Diego (two days of which were presented by Huntley et al., 1981) and on seven days at Leadbetter Beach, Santa Barbara. At both beaches, on all days, improved (higher resolution) wavenumber–frequency spectra indicated that approximately 50% to 90% of the longshore current variance at both arrays is low mode edge waves. The cross-shore current spectra are dominated by unresolvable high mode edge and/or leaky waves, although the low modes are sometimes detectable. In section 5 it is shown that low mode ($n \leq 2$) edge wave elevation variances at the shoreline of both beaches account for roughly 50% of the total variance of the shoreline elevation field (measured with a run-up meter). Daily fluctuations in edge wave shoreline elevation variance levels are found to be well correlated with daily wind wave variance levels at Santa Barbara, but not at Torrey Pines. Lastly, deviations of the field bathymetry from a plane slope and the presence of mean longshore currents have small but detectable effects on the measured dispersion curves (section 6).

2. The field sites

Field measurements were made at two California beaches. Measurements at Leadbetter Beach, Santa Barbara were made in February, 1980. Leadbetter Beach is a 1500 m-long, south-facing pocket beach, bounded to the east by Santa Barbara harbor and to the west by a short headland. A typical profile (Fig. 1)

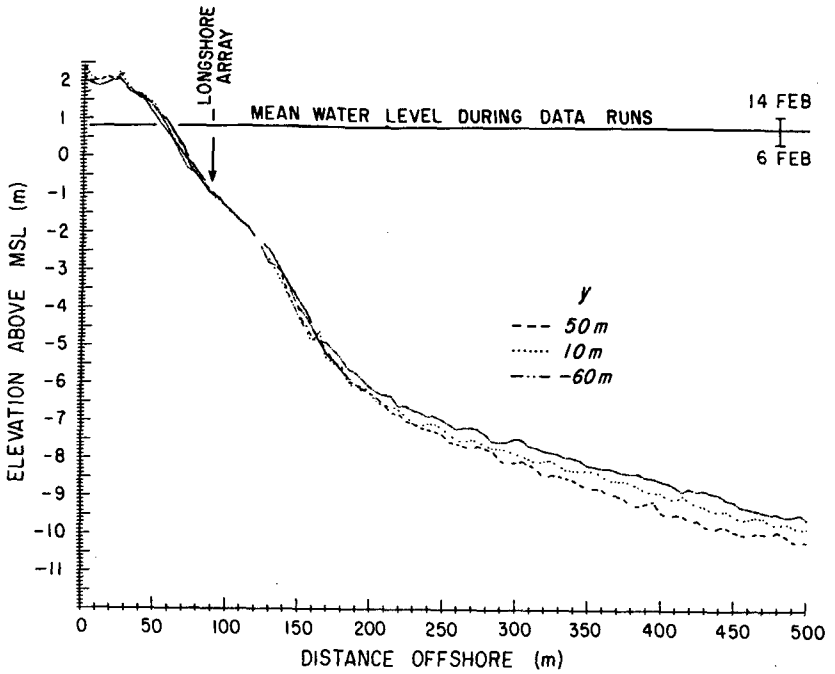

FIG. 1. Beach profiles from three different longshore locations at the Santa Barbara field site.

has a 0.045 plane beach slope out to 2 m below mean sea level (MSL), steepening to 0.06 and tapering off to 0.01 at 7 m below MSL. The incident wind wave field is restricted directionally to two deep water narrow apertures because of the offshore Channel Islands. The fetch between Santa Barbara and the Channel Islands is too short (50 km) for local generation of long gravity waves. The propagation directions of waves passing through the west and southeast windows differ by 100 degrees in deep water (Oltman-Shay and Guza, 1984, Fig. 10). Typically, low frequency energy is expected from the west window and high frequency energy from either the west or southeast windows, dependent on local wind conditions. A 190 m long array of six Marsh-McBirney bidirectional, electromagnetic current meters (4 cm probe diameter) was deployed on a longshore line in the surf zone (Fig. 2). The data were sampled at 64 Hz, low-passed filtered and reduced to 2 Hz. The sensors, data acquisition system and experimental site are fully described by Gable (1981).

Measurements at Torrey Pines Beach, San Diego were made in November 1978. Torrey Pines is a 3 km long, west-facing sandy beach with a reasonably straight shoreline and plane beach slope (approximately 0.02) met by a steeper foreshore slope (approximately 0.04) above mean sea level (Fig. 3). The incident wind wave

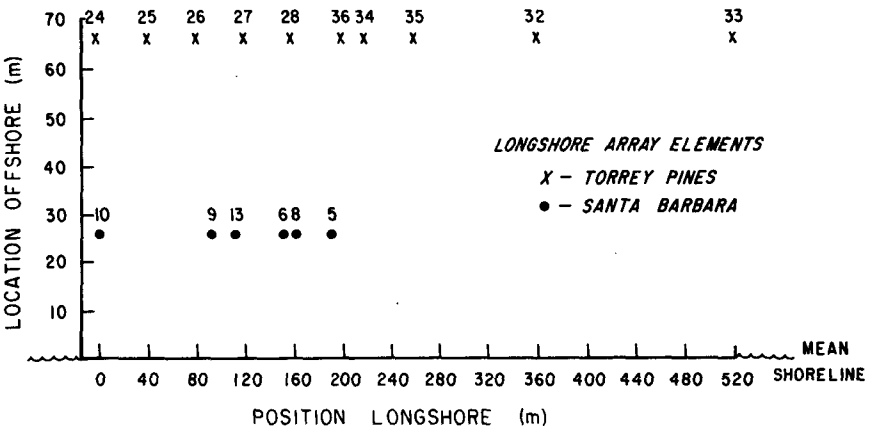

FIG. 2. Plan view of the instrument positions at the Santa Barbara (●) and Torrey Pines (×) field sites.

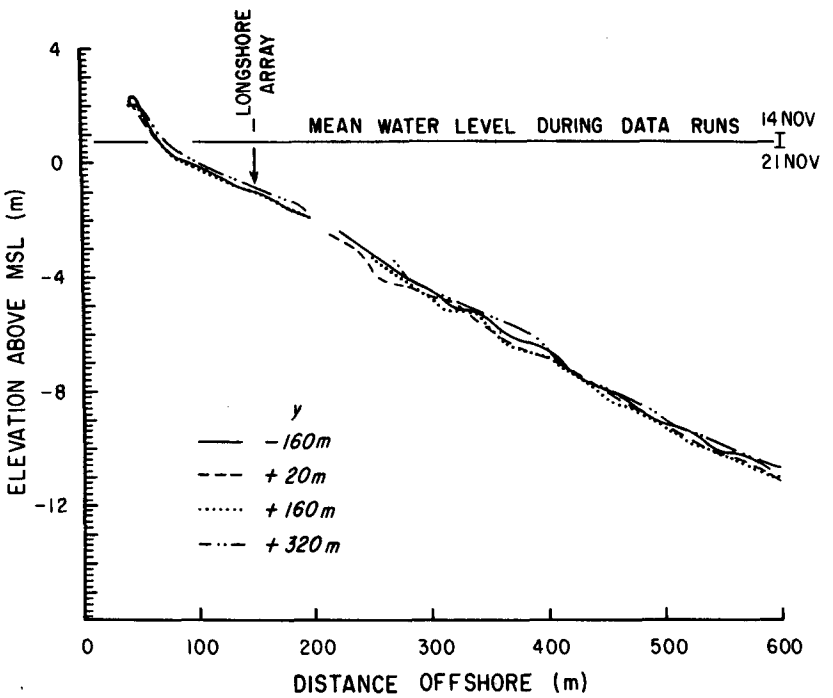

FIG. 3. Beach profiles from four different longshore locations at the Torrey Pines field site.

field is typically directionally bimodal with north and south components due to refraction around the offshore Channel Islands (Pawka, 1982). A 520 meter array of ten current meters was deployed on a longshore line in the surf zone (Fig. 2). The data acquisition scheme was the same as Santa Barbara. The sensors and data files used, and distances of the array from the still water line are given in Table 1.

3. High resolution spectrum estimation

The longshore wavenumber spectrum for each frequency can be determined from the spatially lagged frequency cross-spectrum $[M(\zeta, \sigma)]$ by the relation,

$$E(\sigma, k) = \int M(\zeta, \sigma) \exp(-ik \cdot \zeta) d\zeta \qquad (2)$$

where $E(\sigma, k)$ is the spectral value at the radial frequency σ and longshore wavenumber k and ζ is the longshore spatial lag. However, the cross-spectrum can be measured only at the discrete lag separations of the sensors in the longshore array. The complex cross-spectral data matrix $[M_{ij}(\sigma)]$ for each frequency band is

$$M_{ij}(\sigma) = F_\sigma\{v(x, y_i, t)\} F^*_\sigma\{v(x, y_j, t)\} \qquad (3)$$

where $F_\sigma\{\ \}$ is the complex Fourier coefficient, at frequency σ, of the time series of the velocity component, v, at the cross-shore and longshore locations x, y_i and x, y_j. The asterisk denotes complex conjugate. A discrete Fourier spatial decomposition of this data matrix is not fruitful here because the present arrays are not long compared to the wavelengths of interest. It is therefore necessary to use high resolution methods. One such method is the maximum likelihood estimator (MLE) used by Huntley et al. (1981). Two additional methods are employed here: 1) an iterative form of the

TABLE 1. Summary of data from Santa Barbara (1980) and Torrey Pines (1978). Offshore locations are relative to the still water line as determined by sea level measurements outside the surf zone.

Date	Files*	Cross-spectrum DOF	Missing sensors (number)	Mean offshore location of array (m)
31 Jan 80	1–44	42	None	28
2 Feb 80	33–68	34	5	26
4 Feb 80	9–52	42	None	28
5 Feb 80	2–57	54	8	26
6 Feb 80	1–60	58	None	24
10 Feb 80	1–44	42	None	24
14 Feb 80	1–40	38	9	42
4 Nov 78	1–56	54	33	76
10 Nov 78	1–52	50	None	62
11 Nov 78	10–57	46	None	71
14 Nov 78	4–59	54	None	79
18 Nov 78	2–49	46	24	77
19 Nov 78	4–51	46	None	67
20 Nov 78	5–40	34	26	69
21 Nov 78	2–42	40	26	61

* 1 file = 256 sec, file numbers refer to NSTS data tapes available through sources given by Gable (1981).

MLE, the iterative maximum likelihood estimator (IMLE), and 2) two versions of a minimum weighted window estimator (MWWE) that weights the estimator's wavenumber window according to an a priori estimate of the true spectrum's energetic regions. The two MWWE use different a priori estimates. The MWWE/Th assumes the energy is uniformly distributed at wavenumbers less than and equal to a conservative guess of the mode 0 wavenumber. The MWWE/IML uses the IMLE spectral estimate to identify energetic wavenumbers. The MLE, IMLE and MWWE are linear estimators of $E(\sigma, k)$, having the form

$$\hat{E}(\sigma, k) = \sum_i \sum_j \alpha_{ij}(\sigma, k) M_{ij}(\sigma)$$

where $\alpha_{ij}(\sigma, k)$ are complex variable weights. They have been used as wind-wave directional estimators (Davis and Regier, 1977; Pawka, 1982, 1983). Comparative derivations of the three estimators are given in Oltman-Shay (1985).

The estimated spectrum will vary from the true spectrum because of statistical and instrumental noise in the measured M_{ij} data matrix and inadequate sampling of the spatial lag space. An example of estimator performance on simulated longshore current data is shown in Fig. 4. The true spectrum displays the longshore velocity wavenumber content, at the Santa Barbara array, of a progressive edge wave field containing the first eight modes with equal shoreline elevation amplitude. The longshore (v) current signals of the progressive edge waves at the arrays' offshore locations were simulated using Eckart's (1951) shallow water solution

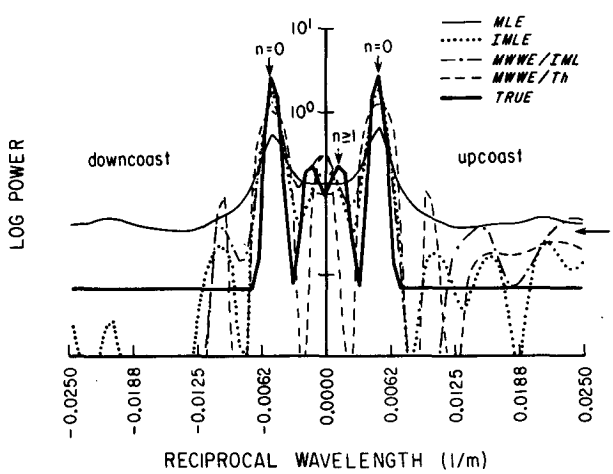

FIG. 4. The true and estimated wavenumber spectra at 0.019 Hz from a simulated longshore velocity signal 26 meters offshore (β = 0.045). The true velocity signal contains the first eight up- and downcoast progressive modes with equal shoreline elevation (broadband noise to signal ratio, NSR = 0.1). Horizontal arrows are the IMLE noise floor. Cross-spectra (DOF = 40) were generated using an array geometry identical to the Santa Barbara array.

$$v(x, y, t) = \frac{a_n g k}{\sigma} L_n(2kx) e^{-kz} \sin(ky - \sigma t) \qquad (4)$$

where a_n is the shoreline elevation amplitude of a mode n edge wave; L_n is a nth order Laguerre polynomial and $\sigma^2 = gk(2n + 1)\tan\beta$. The x (cross-shore) axis origin is at the shoreline and is increasing seaward. Eckart's cross-shore (u) current and elevation solutions are

$$u(x, y, t) = \frac{a_n g k}{\sigma} \frac{\partial}{\partial(kz)} [L_n(2kz) e^{-kz}] \cos(ky - \sigma t)$$

$$\eta(x, y, t) = a_n L_n(2kx) e^{-kz} \sin(ky - \sigma t). \qquad (5)$$

For ease of physical interpretation, the abscissa in Fig. 4 and all subsequent plots are in units of reciprocal wavelength (i.e., $k/2\pi$).

The true wavenumber spectrum in Fig. 4 is dominated by both up and downcoast progressive mode 0 edge waves with less energetic higher modes ($\geq$1) appearing as two low wavenumber peaks. The estimation of the mode 0 peak wavenumber locations by all four estimators is excellent. However, the shape of the peaks differ among the estimators. For instance, the MLE gives a much broader and lower level estimate of the true mode 0 peaks. Examination of estimator response to synthetic test spectra (Oltman-Shay, 1985) shows that the IMLE has the most accurate estimate of a peak's half-power wavenumber bandwidth, as well as the power contained within both its half-power bandwidth and its full breadth (defined from spectral valley-to-valley). The IMLE estimate of a peak's half-power bandwidth and the power contained within that band was on average found to be overestimated by 35% and 20% respectively. Its total peak power (valley-to-valley) estimate, however, was accurate to within 1% (Table A1, NSR = 0.1).

The IMLE and two MWWE spectra portray the true uniform broadband noise floor as numerous peaks (Fig. 4) which are artifacts of window leakage from energetic wavenumbers. The amount of leakage at a wavenumber depends upon the spectrum estimator and the array geometry. For purposes of field data analysis, a noise floor is defined below which all peaks are assumed artificial and therefore ignored. The method of defining the noise floor level in this paper was a two-step process. First, a mean peak energy level was determined from all peaks in the wavenumber spectrum. Second, a new mean peak energy level was calculated for all the peaks below the first mean peak level. This low peak mean level plus its standard deviation was defined as the level of the noise floor. The IMLE noise floor is indicated by a horizontal arrow on Figs. 4 and 6. This "filtering" scheme prejudices our view of the spectrum. No information from a broadband spectrum, other than an absence of peaks, will be extracted. However, it is a necessary convenience when dealing with the field data shown in the next sections; the wavenumber spectra are dominated by a few energetic peaks with numerous

low level peaks which test spectra have shown cannot be confidently identified as real (Oltman-Shay, 1985).

The estimators are applied here to a normalized cross-spectral matrix (diagonal elements are unity). The normalization of matrix elements by the power spectrum removes error in sensor calibration (Munk et al., 1964). A frequency bin width of 0.00195 Hz was chosen in a trade-off between resolution and statistical stability. This selected bin width resulted in approximately 40 degrees of freedom. The wavenumber bin width was dictated by a trade-off between resolution (which should be smaller than the expected wavenumber spread along the edge wave dispersion curves due to the frequency bin width) and computational speed. A wavenumber bin width of 0.0005 m^{-1} was chosen for the Torrey Pines synthetic and field data and 0.00065 m^{-1} for Santa Barbara.

All four estimators were applied to the field data presented here. Their wavenumber spectra were never found to differ appreciably. However, because the IMLE demonstrated superior estimation of half-power bandwidth and peak power, it is used as the primary estimator for the field data. More detailed examples of the IMLE estimator response to synthetic test spectra are in appendix A.

4. Wavenumber–frequency spectra at two beaches

Seven days (spanning a 15 day period) of data from Santa Barbara have been analyzed. The days were chosen for their comparable good data quality. The IMLE estimated wavenumber–frequency (k–f) spectra of longshore and cross-shore currents on 10 February are shown in Fig. 5. This two-dimensional presentation of k–f spectra is designed to address the following questions: 1) Do wavenumber peaks lie on the edge wave dispersion curves? 2) If so, how tightly contained about the dispersion curves is the peak energy? 3) What percent power of the frequency bin lies on and about the dispersion curves?

The dispersion curves for all edge wave modes drawn on the k–f spectra are based on the plane beach dispersion relation [Eq. (1)]. Daily "ridge-fit beach slopes" at Santa Barbara were calculated from Eq. (1) and the observed wavenumbers and frequencies of the mode 0 peaks in the 0.013 to 0.025 Hz band. Therefore, the beach slope used in the mode 1 and higher dispersion curves is inferred from the ridge fit of the mode 0 edge waves. The relationship between the "ridge-fit beach slopes" and the actual topography is discussed in section 6. The k–f figures display the wavenumber space

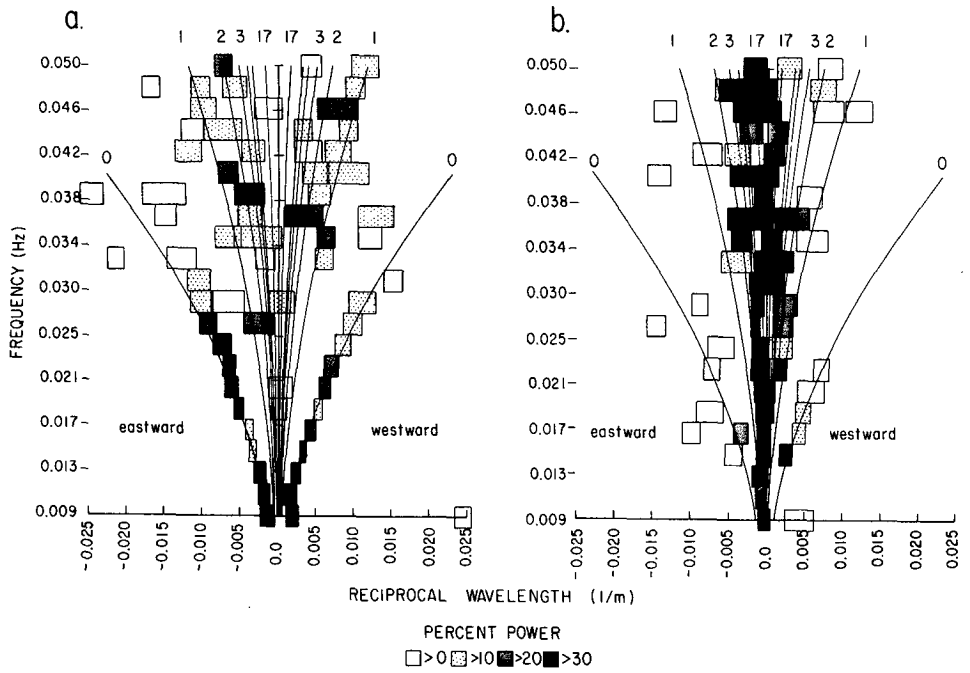

FIG. 5. The (a) longshore and (b) cross-shore current IMLE wavenumber–frequency spectra (DOF = 42) on 10 February 1980 at Santa Barbara. The first four and cutoff mode (17) dispersion lines are drawn for a ridge-fit beach slope $\beta = 0.046$. The rectangular boxes mark the location of energy peaks defined as those wavenumber maxima that have an adjacent valley below their half-power. The wavenumber width of each box is the half-power bandwidth of the peak. The shading density indicates the percent power in the frequency bin that lies within the half-power bandwidth of the peak.

out to 0.025 m^{-1}, although the array at Santa Barbara has a Nyquist wavenumber of 0.05 m^{-1}. There were only a few isolated, very low power peaks beyond 0.025 m^{-1} on all days analyzed.

Figure 6a, b are the four estimated wavenumber spectra for the 0.017 Hz frequency bin in Fig. 5a, b, respectively. The peak locations and half-power bandwidths of the IMLE estimate above the noise floor arrow (section 3) were used to characterize the wavenumber distribution of variance at this frequency in the k–f spectra of Fig. 5.

Eight days (spanning a 17-day period) of data from Torrey Pines have been analyzed. Figure 7 shows longshore and cross-shore current k–f spectra typical of Torrey Pines. Ridge-fit beach slopes were chosen for each day analyzed at Torrey Pines using the dispersion relation and the wavenumber locations and frequencies of the mode 0 and 1 peaks in the 0.007 to 0.027 Hz band. As for Santa Barbara, mode 2 and higher dispersion curves are inferred from the observed mode 0 and 1 edge waves.

All 15 days examined at both beaches display the same dissimilarity in the longshore and cross-shore current k–f spectra as shown in Figs. 5 and 7. The cross-shore current suggests high mode or leaky ($k <$ edge-wave cutoff mode) wave dominance, with some energy appearing on the low-mode dispersion curves at the lower frequencies (Figs. 5b and 7b). The longshore current variance is largely confined to the low mode edge wave dispersion curves (Figs. 5a and 7a).

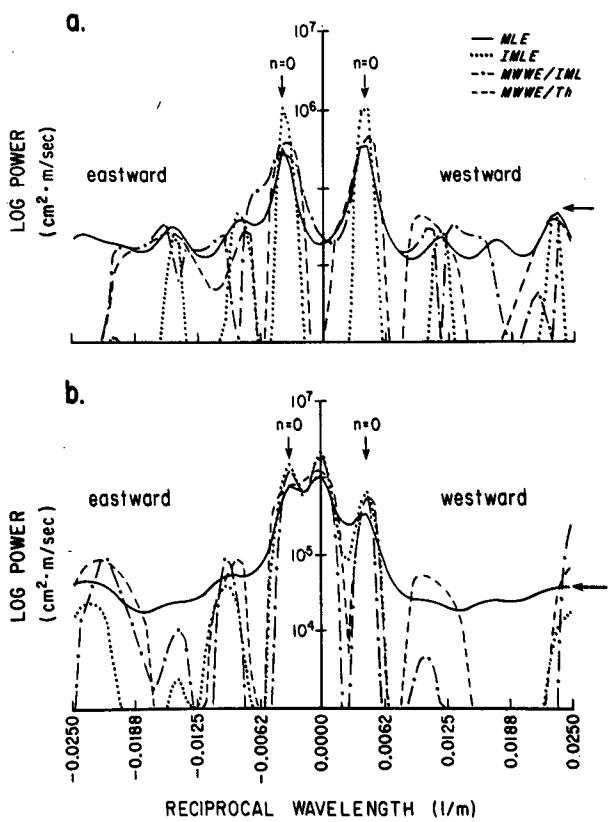

FIG. 6. Four wavenumber spectra estimates (DOF = 42) of the (a) longshore and (b) cross-shore current at 0.017 Hz on 10 February 1980 at Santa Barbara. Vertical arrows mark the wavenumber location of the mode 0 edge wave with $\beta = 0.046$. Horizontal arrows show the IMLE noise floor.

The transition to higher modes with increasing frequency in the longshore current spectra was also observed on all days at Santa Barbara and Torrey Pines. This mode transition is associated with the seaward decay of edge waves. Edge waves have an exponentially decaying cross-shore standing structure of nodes and antinodes which depend on frequency, mode number and beach slope [Eqs. (4) and (5)]. At a fixed offshore location, this structure can result in power fluctuations as a function of frequency (Fig. 8). Modes greater than zero have one or more energy peaks with valleys that mark the frequency at which a node in the cross-shore standing structure is at the array. Higher frequencies are most strongly trapped along the shoreline, yet have larger shoreline velocity amplitudes for the same shoreline elevation amplitude. For instance, the longshore velocity of a mode 0 edge wave can be written as

$$v(x, y, t) = \frac{a\sigma}{\beta} e^{-(\sigma^2/g\beta)x} \sin(ky - \sigma t). \qquad (6)$$

The frequency locations of the transitions from mode zero to higher modes observed in the longshore current spectra at Santa Barbara (0.033 Hz) and Torrey Pines (0.014 Hz) (Figs. 5a and 7a) are in excellent agreement with the transition frequencies shown in Figs. 8a, c (i.e., where mode 0 equals mode 1). The 0.032 Hz transition from mode 1 to higher at Torrey Pines (Fig. 7a) also agrees with Fig. 8c. Figure 8a–d are robust descriptions of the offshore mode energy as a function of frequency. For instance, if mode 1 had twice the shoreline elevation amplitude of mode 0, the transition frequency would shift down less than 0.002 Hz at Santa Barbara (Fig. 8a) and 0.001 Hz at Torrey Pines (Fig. 8c).

In addition to predicting transition frequencies, Fig. 8 suggests that spectral valleys will exist if waves other than mode zero are significant. However, this cannot be observed in the k–f spectra of Figs. 5 and 7 because relative power for each frequency bin is displayed. Figure 9b, d shows that the predicted frequencies of edge wave nodes for cross-shore currents agree well with the observed spectral valleys. The longshore current power spectra and predicted node locations show less agreement (Fig. 9a, c). Here, the valleys coincide with the mode transition frequencies identified in the k–f spectra (Figs. 5a, 7a).

The low mode edge wave information obtained from the longshore velocity spectra are summarized in Tables 2 and 3. Discussion of the percent of the velocity power at the array attributable to a single mode is restricted to subsets of the infragravity band where that

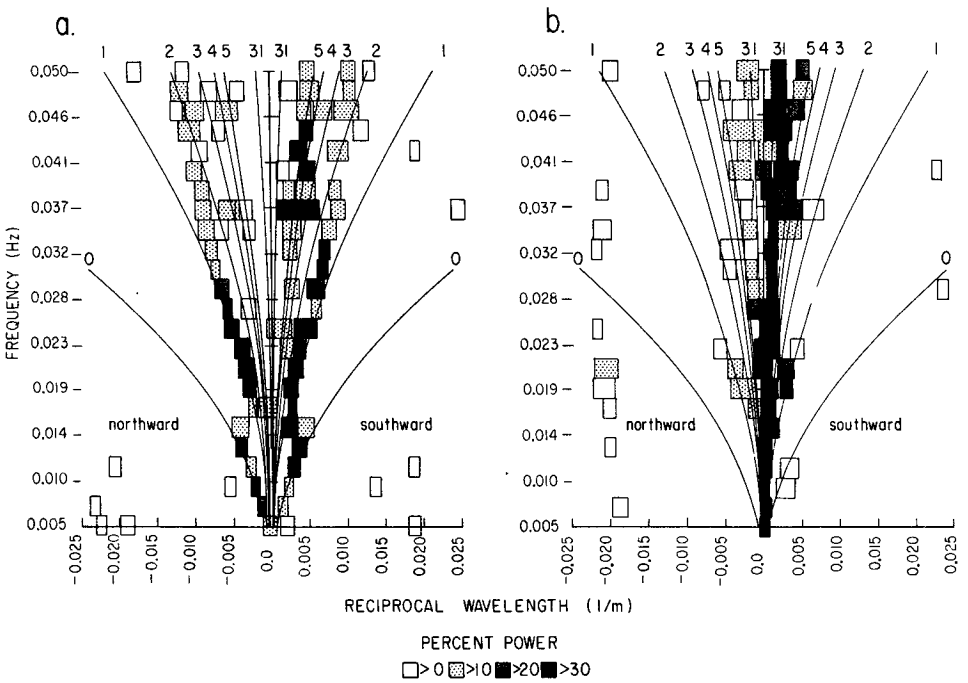

FIG. 7. The (a) longshore and (b) cross-shore current IMLE wavenumber–frequency spectra (DOF = 54) on 4 November 1978 at Torrey Pines. The first six and cutoff mode (31) dispersion curves are drawn for β = 0.025. See Figure 5 for further description.

mode has a strong signal on all days. For instance, Table 2 lists the percent of mode 0 variance contained in the longshore velocity signal at Santa Barbara in the 0.013 to 0.025 Hz band; the lower limit is set by the resolution capabilities of the array and the upper limit by the extent of the mode 0 seaward decay at that frequency relative to mode 1 (Figs. 5a and 8a). Between 70% and 88% of the longshore current variance on all days at the Santa Barbara array in this band is identified as mode 0. The relative amounts of eastward and westward mode 0 progressive waves do not differ appreciably. However, the longshore current in the 0.038 to 0.05 Hz band (identified as 45% to 84% mode 1) shows strong asymmetry in the amount of eastward and westward progressive waves; 5 and 6 February show respectively 2.3 and 3.0 times more energy traveling eastward while 14 February shows 2.5 times more energy traveling westward.

A few days at Torrey Pines exhibit strong asymmetry in the amount of northward and southward progressive edge waves (Table 3). On 10 November, more energy travels southward throughout the longshore current infragravity band while on 20 November, more energy is traveling northward. The eight days of Torrey Pines data show 42% to 79% of the longshore current variance at the array as mode 0 in the 0.007 o 0.011 Hz band, 52% to 77% as mode 1 in the 0.017 to 0.027 Hz band and 48% to 74% as modes 2 and 3 in the 0.037 to 0.05 Hz band.

At both beaches, the percentages of the measured cross-shore current variance at the arrays inferred to be mode 0 are variable: 16% to 48% at Santa Barbara (0.013–0.025 Hz) and 6% to 19% at Torrey Pines (0.007–0.011 Hz) (Tables 2 and 3). The inferred percentages of cross-shore variance in the mode 1 (0.017 to 0.027 Hz) band at Torrey Pines are lower: 3% to 6%.

On 31 January, 48% of the cross-shore current variance at the array in the 0.013 to 0.025 Hz band is inferred to be mode 0 (Table 2). The cross-shore current k–f spectrum from this day shows the low mode edge waves better than any other day (Fig. 10b). To quantify the mode mix of the cross-shore current, the k–f spectra were divided in "low" (modes 1, 2) and "high" (modes greater than 2 and leaky) wavenumber regions. Model testing has indicated that signals of near equal strength that are close in wavenumber space will have confused IMLE peak wavenumber locations. The estimated peaks shift towards one another relative to the true peak locations, with the weaker peak shifting more toward the stronger (Oltman-Shay, 1985). Thus, only a crude description of the energy contained in "low" and "high" mode regions is possible.

The percent of the total variance contained in low and high wavenumber bands, in frequency bands chosen to allow resolution of mode 2 from 3 and to avoid zero crossings, are given in Table 4. Mode 0 is not included because it has significantly decayed at these

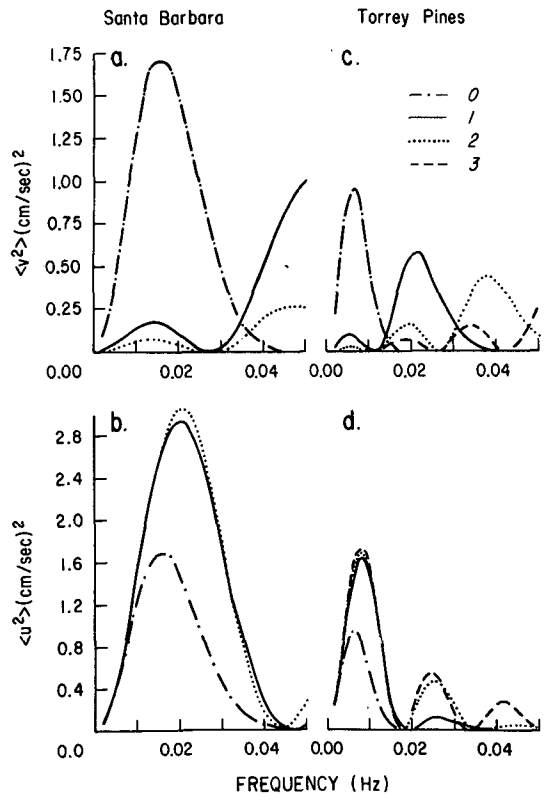

FIG. 8. Simulated velocity variances (at the arrays), as a function of frequency, of edge wave modes with 1 cm shoreline elevation. The (a) longshore, (b) cross-shore current at Santa Barbara (10 February, $x = 24$ m, $\beta = 0.046$) and the (c) longshore, (d) cross-shore current at Torrey Pines (4 November, $x = 76$ m, $\beta = 0.025$).

frequencies. Consistent with Tables 2 and 3, high modes and/or leaky waves contribute substantially to the total cross-shore velocity variance at the array position. The cross-shore currents at the Torrey Pines array show a smaller percent of low mode energy than at Santa Barbara. However, Fig. 8b, d suggest this may be an artifact of the array location and frequency band analyzed. The sum of the percent power in low and high wavenumber bands ranges between 60%–90%, with an average of 73% at Santa Barbara and 85% at Torrey Pines. The remainder of the variance is at wavenumbers greater than mode 1. The relative contribution of decayed mode 0 energy, instrumental and statistical noise is unknown.

The distribution of energy within low and high wavenumber bands of the cross-shore velocity field is given in Table 4 as the wavenumber moment where

$$\text{Wavenumber moment} = \frac{\sum_k kE(\sigma, k)}{\sum_k E(\sigma, k)} \qquad (7)$$

and the summations are over the low or high wavenumber band. All 15 days show low mode energy distributed evenly about modes 1 and 2 in their respective frequency bands (Table 4). The high mode/leaky energy, however, appears relatively more leaky on some days than others (i.e., 31 January compared to 14 February). Their cross-shore current spectra also indicate a dissimilar mode mix (Figs. 10b and 11b).

The longshore current spectra on 14 February show an unusually clear mode-1 edge wave signal in the 0.03 to 0.05 Hz band (compare Figs. 11a with 5a and 10a). This may be a result of a relatively more energetic mode 1 (Fig. 9a). The frequency location of the mode 0 to mode 1 edge wave energy transition is also unusual for Santa Barbara, occurring at a lower frequency. The longshore array is 42 meters from the mean shoreline location of the data run on this day, whereas the other 6 days are 26 ± 2 meters offshore (Table 1). This difference in array location agrees with the lower transition frequency as predicted by the edge wave cross-shore standing structure for longshore current. In addition, the first cross-shore current edge wave node for this array location occurs within the 0.027–0.037 Hz band examined in Table 4, explaining the relatively low percentage (29%) of the cross-shore current variance identified as "high" mode on this day.

The strong mode 0 and 1 longshore current signal on 14 February (Fig. 11a) provides a good opportunity to verify the estimated k–f spectra with the observed cross-shore structure of the longshore current variance (Fig. 12). A cross-shore array of 8 current meters, located in about the center of the longshore array, is used for this purpose. At 0.017 Hz, the cross-shore structure of longshore current variance (Fig. 12a) agrees well with the mode 0 energy observed by the longshore array. At 0.038 Hz, the cross-shore structure (Fig. 12b) does not contradict the mode 1 energy observed by the array. Utilization of cross-shore structure information is difficult, particularly if the edge wave field contains more than one mode (Snodgrass et al., 1962). Furthermore, any mode mix inferred from cross-shore structure will be sensitive to errors in a) sensor calibration, b) sensor location and c) the theoretical cross-shore structure of the velocity potential on real topography (Guza and Thornton, 1985). Nonetheless, Guza and Thornton have been able to demonstrate that on all days discussed here, the cross-shore structure of cross-shore velocity variance and phase is qualitatively consistent with high mode edge and/or leaky waves. However, Guza and Thornton also note that their observations of cross-shore velocity decayed somewhat faster than a pure leaky wave, suggesting the presence of low mode energy.

Figure 13 is a longshore current k–f spectrum extended in frequency to include directionally narrow swell waves ($f \sim 0.06$ Hz) out of the southwest window (section 2). The k–f spectrum above 0.055 Hz shows a concentration of energy on the border of the leaky wave continuum of the eastward-propagating quadrant. The deep water approach angle of these waves is very large

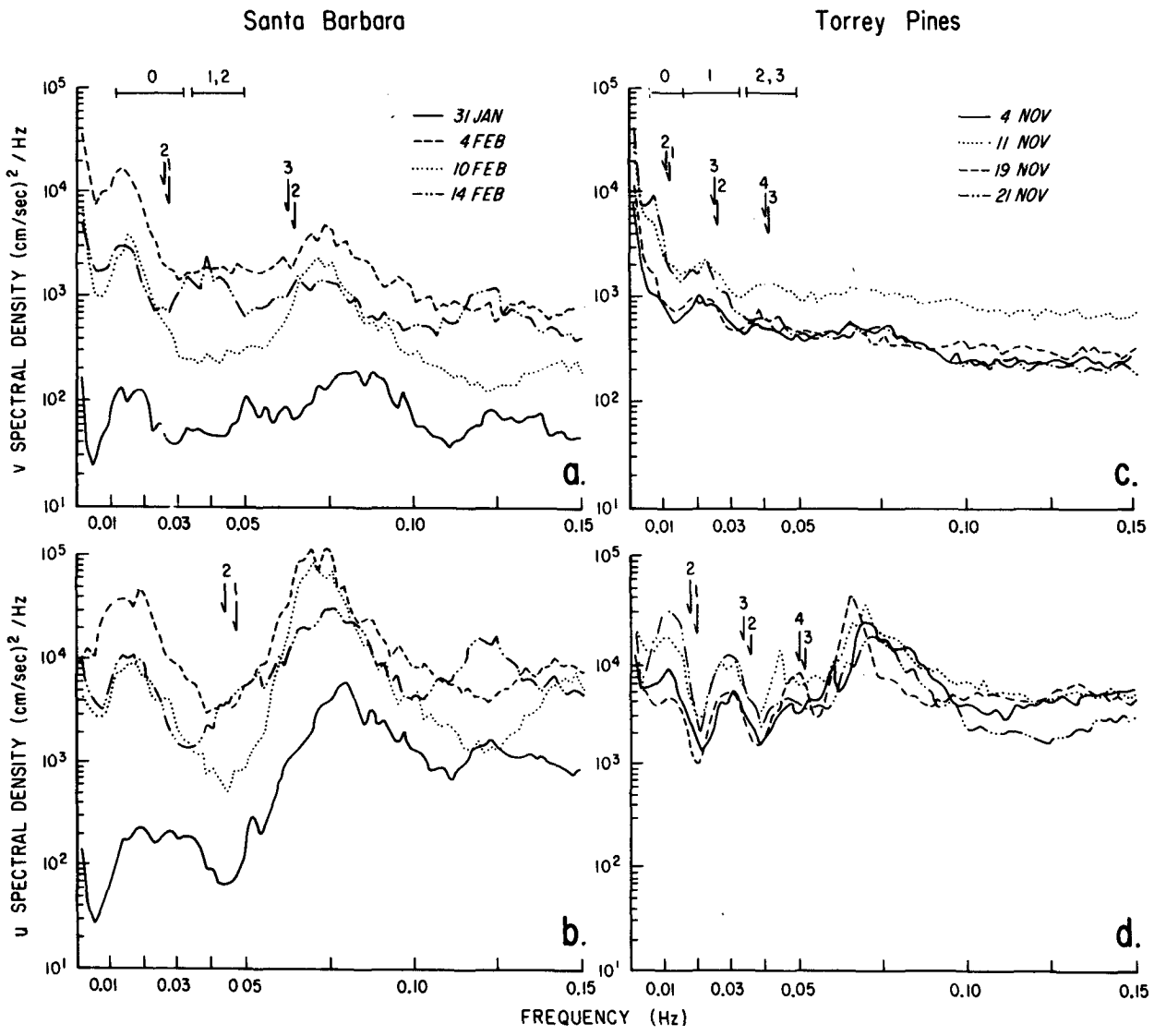

FIG. 9. Typical velocity power spectra (averaged over all array sensors on each day) at Santa Barbara (a) longshore, (b) cross-shore velocity and at Torrey Pines (c) longshore, (d) cross-shore velocity. Vertical arrows mark the expected low mode number frequency nodes. Horizontal bars on (a, c) are observed mode transition frequencies.

(section 2), so the energy is expected to lie very close to the cutoff mode which marks the division between high angle leaky waves and edge waves.

5. Edge wave energy at the shoreline

Shoreline elevation variances of edge wave modes were estimated (Table 5) using the theoretical cross-shore structure (Eqs. 4 and 5) and the k–f spectra obtained from the offshore array observations. On four days at each beach, the total (summed over all k) shoreline elevation variance in corresponding frequency bands were measured with a run-up meter (Table 5). The percent contributions of different edge-wave mode numbers to the total shoreline elevation variance, within the same frequency bands, are given in Table 6.

At Santa Barbara, the mode 0 edge wave contribution to the total shoreline elevation variance in the 0.013–0.025 Hz band varies between 20% and 36%. In the adjacent frequency band (0.027–0.037 Hz), the contribution of modes 1, 2, and modes ≥ 3 (and leaky) also vary by less than a factor of 2 (20%–39% and 48%–63%, respectively). The contribution of mode 1 in the 0.038–0.05 Hz band varies by nearly a factor of 5. Unfortunately, run-up data is not available for 31 January when the percent of cross-shore current variance at the array inferred to be mode 0 in the 0.013–0.025 Hz band is nearly double that of all other days (Table 2). On this day, mode 0 could account for 50% of the total

TABLE 2. Summary of the modal contribution to velocity variance at the offshore position of the Santa Barbara array. Ridge-fit beach slopes (β) are based on observed distribution of longshore current variance in k, f space and the edge wave dispersion relation [Eq. (1)]. Longshore current columns are frequency band averaged ratios of up- and downcoast traveling velocity variances within measured k, f peaks (spectral valley to spectral valley), and the percent of the total longshore current variance contained within both peaks. The contributions of the edge wave mode to the total measured cross-shore velocity variance at the array was inferred from the longshore current k, f measurements and Eqs. (4) and (5).

	Ridge-fit beach slopes Mode 0, 0.013–0.025 Hz		Mode 0, 0.013–0.025 Hz Longshore			Mode 1, 0.038–0.05 Hz Longshore	
Date (1980)	Eastward	Westward	Eastward / Westward	% Total	Inferred % cross-shore total	Eastward / Westward	% Total
31 Jan	0.052	0.054	0.8	88	48	0.7	72
2 Feb	0.053	0.052	0.8	79	27	0.6	77
4 Feb	0.053	0.037	0.9	75	22	1.6	45
5 Feb	0.047	0.036	1.1	76	19	2.3	57
6 Feb	0.042	0.036	1.0	68	22	3.0	65
10 Feb	0.048	0.044	0.8	83	25	1.5	64
14 Feb	0.044	0.049	1.1	70	16	0.4	84

shoreline elevation variance, although the surf beat energy levels are very low (Fig. 9a, b).

If mode 0 is assumed to contribute about 25% of the shoreline elevation variance in the 0.027–0.037 Hz band (as it does in the 0.013–0.025 Hz band, Table 6a), then the total contribution of edge wave modes 0, 1, 2, ≥ 3 and leaky waves identified by the offshore array account for 96%–119% of measured shoreline elevation variance in the 0.027–0.037 Hz band.

At Torrey Pines, the contributions of mode 0 and 1 to the total shoreline elevation variance are similar to Santa Barbara (20%–40%) and show comparable fluctuations of about a factor of 2. However, the shoreline elevation amplitudes inferred from the array measurements are less consistent with the run-up measurements at Torrey Pines than at Santa Barbara. The combined contributions of modes ≥ 3 (0.021–0.029 Hz) and mode 1 (0.017–0.027 Hz) excede 100% of the measured shoreline variance on 10 and 19 November (124%, 147% respectively). Any contribution from mode 0 would increase the disparity. Nevertheless, Table 6 suggests that low mode edge waves ($n \leq 2$) constitute about 50% of the infragravity elevation variance at the shoreline of both beaches.

Daily fluctuations in the shoreline elevation variance *density* of individual edge wave modes (within particular frequency bands) were regressed against the variance in the wind and swell wave frequency band (Table 5). All four correlations were statistically significant (95% confidence) at Santa Barbara (Table 7). At Torrey Pines only 1 of the 3 correlations is statistically different from zero. Indeed, theory (Gallagher, 1971) and experiments (Bowen and Guza, 1978) concerning the excitation of edge waves by incident wave groups suggests a dependence of edge wave energy levels on the wavenumber–frequency distribution of incident wave en-

TABLE 3. Summary of the modal contribution to velocity variance at the offshore position of the Torrey Pines array. (See Table 2 for further explanation.).

	Ridge-fit beach slopes Modes 0 & 1, 0.007–0.027 Hz		Mode 0, 0.007–0.011 Hz Longshore			Mode 1, 0.017–0.027 Hz Longshore			Modes 2 & 3, 0.037–0.05 Hz Longshore	
Date (1978)	Northward	Southward	Northward / Southward	% Total	Inferred % cross-shore total	Northward / Southward	% Total	Inferred % cross-shore total	Northward / Southward	% Total
4 Nov	0.025	0.026	1.1	45	6	0.8	75	3	0.7	72
10 Nov	0.023	0.020	0.6	48	15	0.3	61	3	0.5	48
11 Nov	0.024	0.023	1.1	48	13	1.0	52	4	0.8	70
14 Nov	0.029	0.026	1.2	59	19	1.2	77	6	1.5	74
18 Nov	0.022	0.025	0.9	42	6	0.7	70	4	0.5	67
19 Nov	0.024	0.023	1.0	42	13	1.1	63	4	0.7	66
20 Nov	0.023	0.025	2.5	73	17	1.6	52	5	1.4	65
21 Nov	0.021	0.021	0.9	79	17	0.9	50	3	0.9	65

TABLE 4. Percentage of total cross-shore velocity variance and the average reciprocal wavelength moment (= wavenumber moment/2π) of energy contained in low mode edge wave and high mode/leaky wavenumber bands. Calculations based on cross-shore current k-f spectra. The noninteger mode number satisfies the edge wave dispersion relation for the wavenumber moment, the center frequency and the ridge-fit beach slope.

	Modes 1 and 2			Modes 3 to cutoff and leaky		
		Wavenumber moment/2π			Wavenumber moment/2π	
Date	Power %	(m^{-1})	(Mode number)	Power %	(m^{-1})	(Mode number)
1980			Santa Barbara: 0.027–0.037 Hz			
31 Jan	35	0.0034	1.3	48	0.0009	6.4
2 Feb	20	0.0033	1.4	60	0.0009	6.4
4 Feb	32	0.0037	1.5	40	0.0014	4.7
5 Feb	27	0.0040	1.5	46	0.0014	5.1
6 Feb	33	0.0045	1.4	42	0.0013	6.0
10 Feb	30	0.0035	1.5	57	0.0012	5.4
14 Feb	33	0.0037	1.4	29	0.0014	4.5
1978			Torrey Pines: 0.021–0.029 Hz			
4 Nov	14	0.0039	1.5	71	0.0012	6.2
10 Nov	12	0.0044	1.6	75	0.0015	5.8
11 Nov	17	0.0041	1.6	61	0.0013	6.2
14 Nov	19	0.0034	1.6	66	0.0012	5.2
18 Nov	17	0.0040	1.6	71	0.0013	6.2
19 Nov	16	0.0041	1.6	74	0.0011	7.4
20 Nov	15	0.0041	1.6	57	0.0011	7.4
21 Nov	8	0.0044	1.7	79	0.0013	6.8

ergy. Oltman-Shay and Guza (in preparation) show that a model (after Gallagher, 1971) which includes two-dimensional incident wind wave information, can explain (in a statistically significant way) the daily fluctuation in the modal energy at Torrey Pines that is statistically uncorrelated with total wind wave variance.

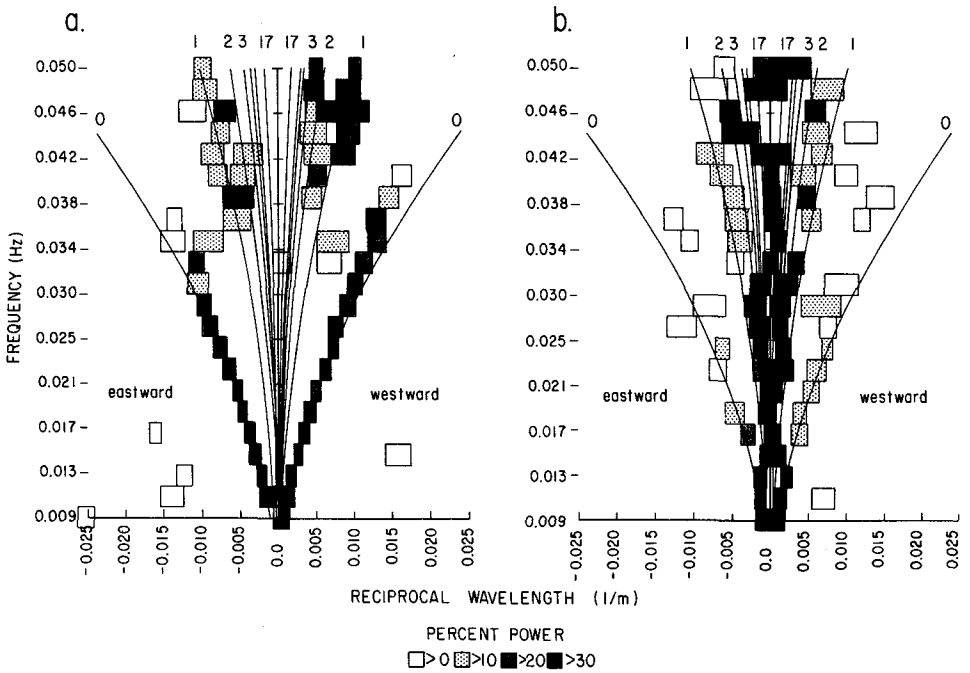

FIG. 10. The (a) longshore and (b) cross-shore current IMLE wavenumber-frequency spectra (DOF = 42) on 31 January 1980 at Santa Barbara. The first four and cutoff mode dispersion curves are drawn for $\beta = 0.053$.

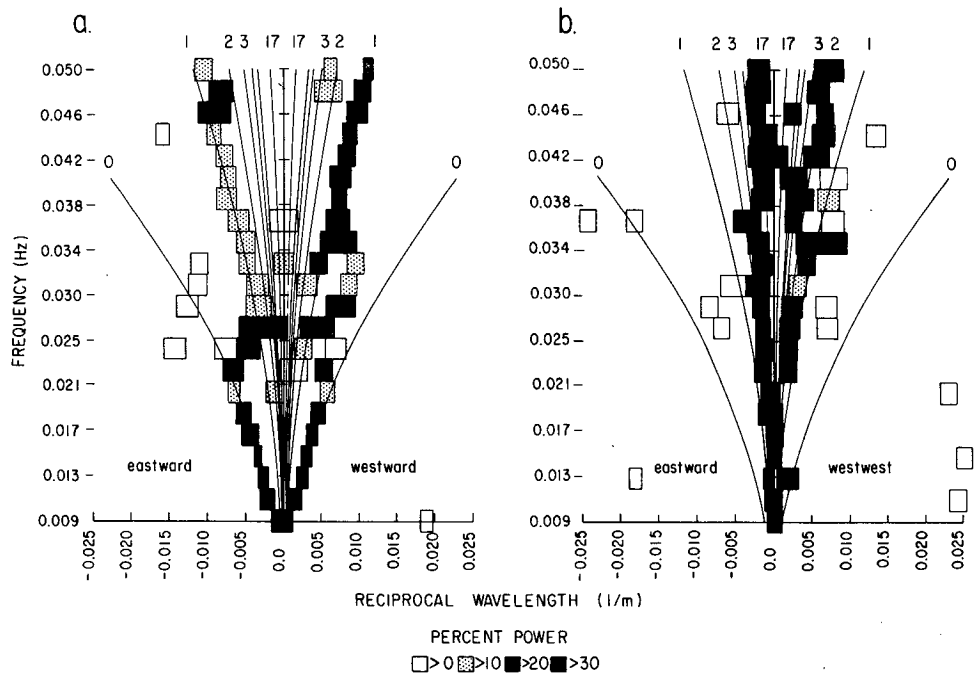

FIG. 11. The (a) longshore and (b) cross-shore current IMLE wavenumber–frequency spectra (DOF = 38) on 14 February 1980 at Santa Barbara. The first four and cutoff mode dispersion curves are drawn for $\beta = 0.046$.

When the sum of edge wave variance densities within similar frequency bands (Torrey Pines: mode 1, 0.017–0.027 Hz and modes ≥ 3, 0.021–0.029 Hz; Santa Barbara: modes 1, 2, 0.027–0.037 Hz and modes ≥ 3, 0.027–0.037 Hz) are regressed against wind wave variance (0.05–0.3 Hz) the correlation is 0.92 at Santa Barbara and 0.34 at Torrey Pines. The slopes of the regression lines, constrained to pass through the origin, are within 30% of 20 Hz^{-1}. If the 20 Hz^{-1} regression slopes for these particular frequency bands are taken as representative of a surf beat band defined as $f < 0.05$ Hz, then total wind wave variance (0.05–0.3 Hz) and surf beat shoreline elevation variance (all k, all $f < 0.05$ Hz) will be equal. This is consistent with the conclusions based on regression between wind wave variances and many days of run-up data; the significant height of the run-up at surf beat frequencies is approximately equal to the significant height of offshore wind and swell waves (Guza and Thornton, 1985).

6. Theoretical dispersion curves

Edge-wave dispersion lines for a plane beach were drawn on the k–f spectra of Figs. 5, 7, 10, 11 and 13 using equation 1 with the average of the ridge-fit beach slopes calculated for up and downcoast waves (section 4). That is, β in Eq. (1) was determined by fitting to the observations. It is shown below that the theoretical dispersion curves, calculated from the observed bathymetry, are very similar to the ridge-fit dispersion curves. However, departures of the mode energy from the ridge-fit dispersion curves are observed and are shown to be associated with beach concavity and occasional strong longshore currents.

Dispersion curves for the measured profiles (Figs. 1 and 3 are typical) were developed using the approximate method given by Holman and Bowen (1979) for concave beaches. Their algorithm provides an excellent approximation to Ball's (1967) analytical solution and compared well with their own numerical results. The longshore current k–f spectra on 14 November at Torrey Pines with ridge-fit and Holman and Bowen (1979) dispersion curves is shown in Fig. 14. The dispersion curves are similar, but the concave beach solution clearly is closer to the observations. The mean water level during 14 November (Fig. 3) was the highest of any Torrey Pines run, so the effect of beach concavity is expected to be maximum on this day. The effect is detectable, but not significant at these length scales and it therefore appears that a plane beach with a ridge-fit beach slope is a reasonable approximation to the true dispersion relation. On days at Torrey Pines with high mean water levels and concomitant concave beach profiles, there is a strong vertical trend to the mode 1 energy in the mode 1 to mode 2 transition region (i.e., Fig. 7, 0.03–0.04 Hz). This trend is consistent with beach concavity which produces a relatively steeper dispersion curve (Fig. 14) and a less decayed mode 1 edge wave at the array in the transition frequency band than on a plane beach. Additionally, the IMLE tends to shift the wavenumber locations of weaker peaks (i.e.,

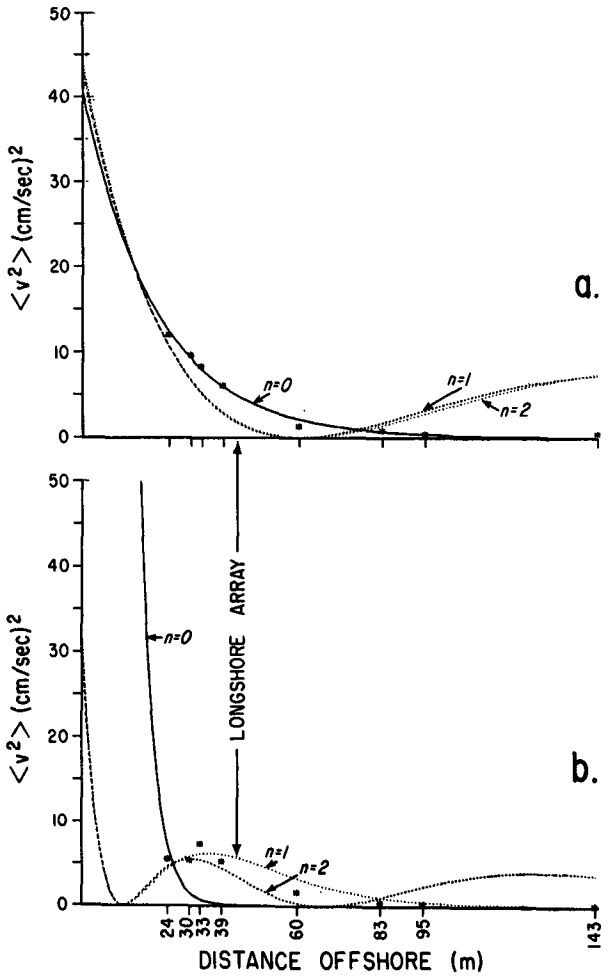

FIG. 12. The longshore current variance at frequencies (a) 0.017 Hz and (b) 0.038 Hz measured at discrete locations offshore (•). Also shown are cross-shore profiles of low mode edge waves, with amplitudes individually determined by a least-squares-fit to the data.

mode 1) towards more energetic peaks (i.e., mode 2) (Oltman-Shay, 1985), also possibly contributing to the apparent vertical ridge in k–f space. The Santa Barbara foreshore beach is less concave than Torrey Pines and deviations from a plane beach are not appreciable.

Longshore currents at Santa Barbara were strong enough to distort the dispersion curves (Fig. 15). The eastward-propagating edge waves on 5 February appear to experience a steeper beach slope than the westward-propagating waves. The magnitude of a steady longshore current needed to create this apparent asymmetry in the up- and downcoast beach slope is estimated below and compared with mean flow observations.

A mean longshore current, $\bar{v}$ causes an increase in the phase velocity of the edge waves

$$C_p + \bar{v} = \frac{\sigma + \delta\sigma}{k} \tag{8}$$

as seen by the fixed sensors. The Doppler shift ($\delta\sigma$) is related to the apparent beach slope asymmetry, $\delta\beta = (\beta^W - \beta^E)/2$, by

$$(\sigma + \delta\sigma)^2 = gk(2n+1)(\beta + \delta\beta)$$

or

$$\delta\sigma = \frac{\sigma\delta\beta}{2\beta} \tag{9}$$

for mode 0. Observed values of $\delta\beta$ from the ridge-fit beach slopes of the mode 0 up- and downcoast propagating waves at Santa Barbara (Table 2) were used to calculate the Doppler frequency shift (Eq. 9) and the concomitant mean longshore current, $\bar{v}$ (Eq. 8) (Table 8). Even this simple, first order look at the Doppler shift and the measured steady longshore currents is reasonably successful. However, a more careful study accounting for the nonuniformity of the current in the cross-shore direction might substantially modify these values.

The edge wave mode peaks in the k–f spectra have wavenumber spread. The average half-power bandwidth of the mode 0 edge waves observed at Santa Barbara and Torrey Pines are $2\pi(0.0018)$ m^{-1} and $2\pi(0.0012)$ m^{-1}, respectively. The continuum of edge wave energy in frequency will contribute to the wavenumber spread. An estimate of this spread is

$$\Delta k = \frac{2\sigma\Delta\sigma}{g\sin(2n+1)\beta} \tag{10}$$

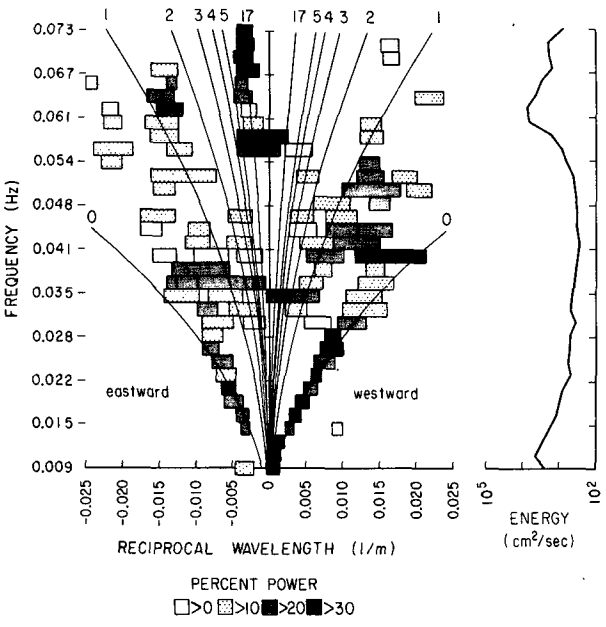

FIG. 13. The longshore current IMLE wavenumber–frequency spectrum (DOF = 34) on 2 February 1980 at Santa Barbara. The first six and cutoff mode dispersion curves are drawn for $\beta = 0.052$. The swell energy around 0.06 Hz (power spectrum averaged over the array sensors is included) is concentrated near the cutoff mode.

TABLE 5. Daily estimates of the edge wave shoreline elevation variance (cm^2) identified by the longshore (Tables 2 and 3) and cross-shore (Table 4) current k–f spectra; the total shoreline elevation variance (cm^2) obtained from the run-up meter; and the offshore wind wave elevation variance (cm^2).

(a) Santa Barbara

	0.013–0.025 Hz		0.027–0.037 Hz			0.038–0.05 Hz		
Date (1980)	Mode 0	Total	Modes 1, 2*	Mode ≥ 3* leaky	Total	Mode 1	Total	0.05–0.3 Hz Wind waves
31 Jan	1.2	—	1.0	1.5	—	0.6	—	32
2 Feb	11	41	8	24	37	8	20	155
4 Feb	76	214	40	56	102	11	57	383
5 Feb	36	144	28	58	119	7	77	216
6 Feb	9	45	12	18	33	4	45	101
10 Feb	16	—	5	10	—	3	—	118
14 Feb	31	—	—	—	—	30	—	415

(b) Torrey Pines

	0.007–0.011 Hz		0.017–0.027 Hz		0.021–0.029 Hz		
Date (1978)	Mode 0	Total	Mode 1	Total	Modes ≥ 3* leaky	Total	0.05–0.3 Hz Wind waves
4 Nov	3	—	17	—	54	—	279
10 Nov	13	36	35	109	90	97	621
11 Nov	12	—	31	—	67	—	1020
14 Nov	6	39	22	76	37	55	371
18 Nov	5	—	19	—	77	—	406
19 Nov	3	15	14	45	44	38	269
20 Nov	22	—	21	—	32	—	398
21 Nov	22	58	21	127	75	110	385

* Values listed are the average of the shoreline elevation estimates for the two extreme mode numbers on days when these estimates differ less than 6% (see Fig. 8).

from the derivitive of the dispersion relation [Eq. (1)]. The present frequency bin width (0.00195 Hz) can account for at least $2\pi(0.0010)$ m^{-1} of the wavenumber spread for both Santa Barbara and Torrey Pines (without accounting for windowing spread). The frequency resolution can be as critical to the resolution of edge wave modes as the array length. Longer spatial arrays would not have improved our low mode wavenumber resolution when constrained to this frequency bin width. However, because high modes experience less wavenumber spread from the frequency continuum [Eq. (10)], a longer array might have improved the separation of the high modes and leaky waves. We note that records as long as eight hours were collected, but the array sensors came out of the water in wave troughs except for a few hours around high tide.

TABLE 6. Percentages of total shoreline elevation variance, within indicated frequency bands, contained in identifiable edge wave modes.

Santa Barbara

Date (1980)	Mode 0 0.013–0.025	Modes 1, 2 0.027–0.037	Mode ≥ 3 leaky 0.027–0.037	Mode 1 0.038–0.05
2 Feb	27	20	64	40
4 Feb	36	39	55	19
5 Feb	25	23	48	9
6 Feb	20	36	53	8

Torrey Pines

Date (1978)	Mode 0 0.007–0.011 Hz	Mode 1 0.017–0.027	Modes ≥ 3 leaky 0.021–0.029
10 Nov	36	32	92
14 Nov	15	29	66
19 Nov	20	31	116
21 Nov	38	17	68

Because the wavenumber resolution is limited by the frequency resolution, only an upper bound on the true half-power bandwidth of the peaks in wavenumber space can be estimated. These typical mode 0 observed half-power bandwidths at Santa Barbara and Torrey Pines correspond to lower bound "Q" estimates ($k/\Delta k$) of 2.9 and 2.0, respectively. The half-power bandwidth of the peaks along a dispersion curve in many longshore current k–f spectra increase with increased frequency (i.e., mode 0, Fig. 5a). Without better frequency resolution, it is impossible to ascertain whether this increase reflects a near constant Q of the resonant system for that mode or increased spreading from

TABLE 7. Results of linear regressions between edge-wave shoreline elevation variance density (cm^2 Hz^{-1}) and total wind and swell wave variance (0.05–0.3 Hz, cm^2). Slopes (and 95% confidence intervals) of the regression lines (R) are given only when the correlation is significant with 95% confidence.

Mode number	Frequency range (Hz)	Correlation	Number of days	R (Hz^{-1})	Site
0	0.013–0.025	0.80	7	12. ± 9.	SB
1, 2	0.027–0.037	0.94	6	12. ± 5.	SB
≥3, Leaky	0.027–0.037	0.88	6	18. ± 11.	SB
1	0.038–0.05	0.85	7	4.9 ± 3.0	SB
0	0.007–0.011	0.23	8	—	TP
1	0.017–0.027	0.80	8	2.4 ± 1.6	TP
≥3, Leaky	0.021–0.029	0.34	8	—	TP

the frequency continuum with increased frequency [Eq. (10)].

7. Discussion

Surf zone infragravity energy at two California beaches was always found to contain detectable edge waves. Most (70%–88%) of the longshore current variance at the Santa Barbara array was identified as mode 0 in the 0.013 to 0.025 Hz band over the seven days studied (Table 2). Higher modes were not observed in the longshore current at these frequencies. Model testing of the spectrum estimators showed that even if higher modes had shoreline elevation amplitudes equal to mode 0, their signal at the array would be relatively too weak to extract (appendix A). Mode 1 (and some mode 2) appeared in the upper infragravity band (0.038–0.05 Hz) of the longshore current spectra (45% to 84% of the variance, Table 2) where mode 1 had a strong longshore current response and mode 0 had decayed (Fig. 8a). The mode 0 shoreline elevation amplitude (inferred from longshore current amplitude at the array) showed some days having had no appreciable variation over the 0.013 to 0.025 Hz band, suggesting frequencies greater than 0.025 Hz may have contained significant mode 0 energy trapped shoreward of the array.

Longshore current variance for eight days at the Torrey Pines array was identified as 42%–79% mode 0 in the 0.007–0.011 Hz band, 61%–77% mode 1 in the 0.017–0.027 Hz band and 48%–74% mode 2 and/

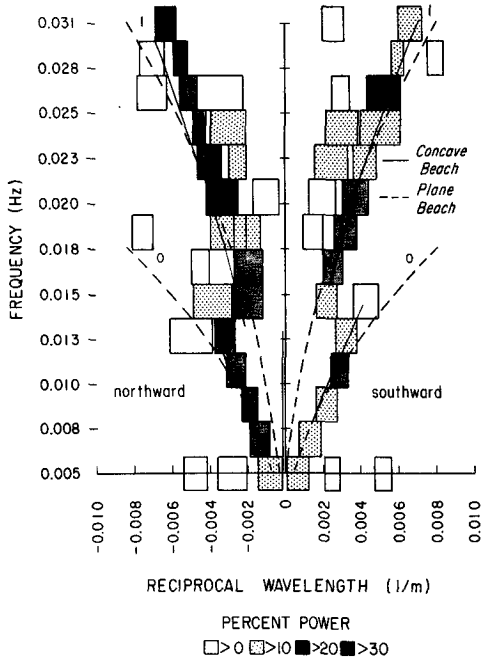

FIG. 14. The longshore current IMLE wavenumber–frequency spectrum (DOF = 54) on 14 November 1978 at Torrey Pines. Mode 0 and 1 dispersion curves are drawn for the measured beach profile (using Holman and Bowen's, 1979, approximation for a concave beach) and for a plane beach with the ridge-fit beach slope (β = 0.0275).

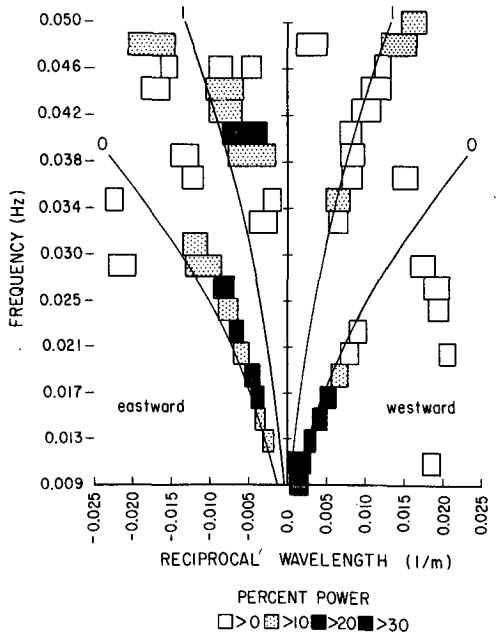

FIG. 15. The longshore current IMLE wavenumber–frequency spectrum (DOF = 54) on 5 February 1980 at Santa Barbara. Mode 0 and 1 dispersion curves are drawn for the average of the up and downcoast ridge-fit beach slopes (β = 0.0415).

TABLE 8. Steady longshore currents measured (average of array sensors) and calculated from the observed Doppler frequency shift at 0.019 Hz in the k–f spectra at Santa Barbara. Positive currents flow from east to west.

	Longshore currents	
Date (1980)	Doppler estimated (cm s^{-1})	Measured (cm s^{-1})
31 Jan	+5	+5
2 Feb	−2	−10
4 Feb	−33	−45
5 Feb	−23	−29
6 Feb	−14	−14
10 Feb	−7	−8
14 Feb	+12	+15

or 3 in the 0.037–0.05 Hz band (Table 3). Similar to Santa Barbara, the single mode domination of a frequency band was explained by the preferential response of the longshore current (for equal shoreline elevation amplitude) to the lowest mode not trapped significantly shoreward of the array (Fig. 8c).

Mode variance in the cross-shore current at the array was inferred from the longshore current estimates. The cross-shore current at Santa Barbara contained 16% to 48% mode 0 variance in the 0.013 to 0.025 Hz band. At Torrey Pines, 6% to 19% was inferred to be mode 0 in the 0.007 to 0.011 Hz band and 3% to 6% inferred as mode 1 in the 0.017 to 0.027 Hz band. The day with 48% of the cross-shore current variance identified as mode 0 (31 January), had the lowest levels of incident wind wave energy (significant height = 22 cm) and surf zone infragravity energy (Fig. 9). The distribution of the cross-shore current variance within the unresolvable low wavenumber band also differed amongst the days analyzed (Table 4), with some days appearing less "leaky" than others.

Longshore current variance was observed to consist primarily of low-mode edge waves. Cross-shore currents also contained low mode edge waves, but were often dominated by low wavenumber energy that probably consisted of a combination of unresolvable high-mode edge waves and/or leaky waves. Because high mode and leaky wave velocities have their largest component in the cross-shore direction at the arrays (Fig. 8), the observation that high modes dominate the cross-shore current does not contradict the longshore current observations of low modes. These data are strongly suggestive of a nearshore infragravity field with comparable shoreline elevation variance in low mode ($n \leq 2$) and high mode and/or leaky wave bands (Table 6).

The possible existence of standing edge waves at Torrey Pines (Huntley et al., 1981) was not addressed. Wavenumber analysis methods used here assume spatial homogeneity. Further work is needed to assess the effect of inhomogeneity on the spectrum estimators before this question can be properly addressed. However, it should be noted that cross-spectra from Santa Barbara does not show the spatial inhomogeneity observed at Torrey Pines (Huntley et al., 1981).

The present observations suggest a more variable picture of the distribution of energy between edge and leaky waves than Munk et al. (1964). Their offshore (500 m) pressure observations, used to generate a single k–f spectrum for the 2 to 60 cph band, extended over many months. They noted, as we have, that the absolute energy of the modes within a frequency band varied from day to day. But, they also observed that the relative mode mix remained constant enough to assume temporal stationarity of the normalized cross-spectra. We observed that mode 0 percent contribution to the total shoreline elevation variance at both beaches varied by about a factor of 2 (Table 6) and that the distribution of the cross-shore velocity variance in k–f space appeared more leaky on some days than others (Table 4). In addition, they observed essentially equal amounts of progressive edge wave energy traveling up- and downcoast while the present observation showed as much as three times more edge wave mode energy traveling in one direction (Tables 2 and 3).

The upper frequencies analyzed by Munk et al., (1964), overlap the lowest frequencies considered here (0.017 Hz = 60 cph). They identified greater than 90% of the energy as modes 0 through 5 at their upper frequencies; the leaky wave continuum contained less than 10% and at some frequencies as low as 2%. The present results identified some mode 0 energy, but unfortunately, could not resolve the higher modes and leaky waves to assess the degree of agreement between the two datasets in this frequency band. In general, modes greater than five (and/or leaky waves) appear to play a more important role in the cross-shore velocity and elevation fields in the surf zone at infragravity frequencies than offshore at lower frequencies.

Acknowledgments. Support for analysis was provided by the Office of Naval Research, Coastal Sciences Branch, under Contract N00014-83-C-0182. The data collection was supported by ONR and the Sea Grant Nearshore Sediment Transport Study (Project Number RICA-N-40). E. B. Thornton played a central role in all phases of the experiments, R. L. Lowe was the principal engineer and R. J. Seymour obtained the bathymetry. Many others contributed to deploying and maintaining the instruments. J. Semler typed the manuscript and M. Clark drafted the figures. A special thanks to Drs. A. J. Bowen, D. A. Huntley and the anonymous reviewers for their insightful and constructive comments.

APPENDIX A

Synthetic Test Spectra

Synthetic cross-spectral matrices were developed from test spectra designed to represent possible edge

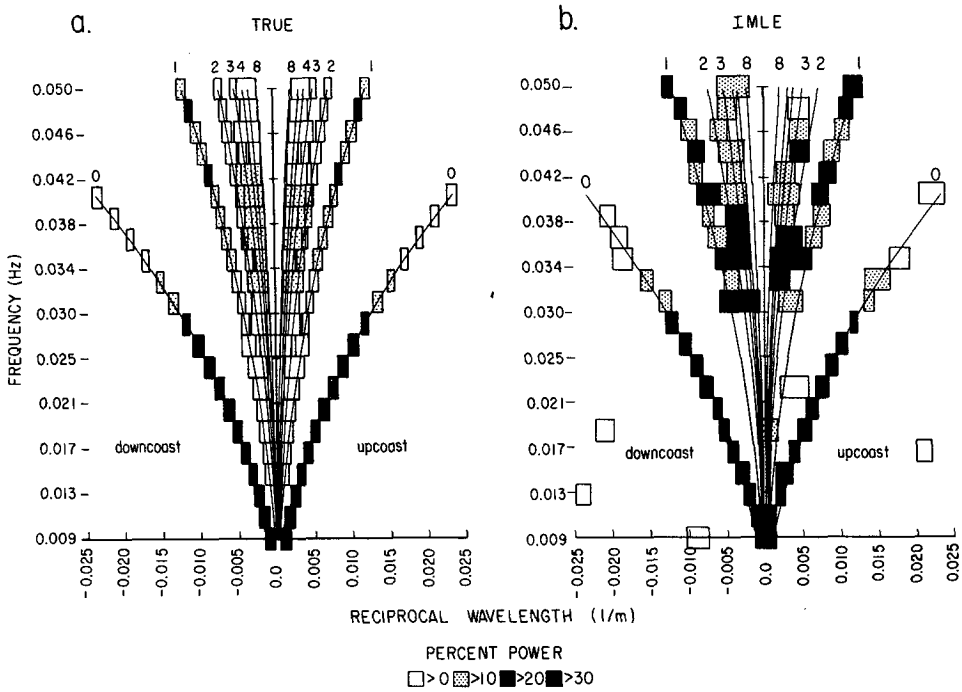

FIG. A1. The true (a) and IMLE estimated (b) wavenumber–frequency spectra from a simulated longshore velocity signal at Santa Barbara (x = 26 m, β = 0.045, DOF = 40). The true velocity signal contains the first eight up- and downcoast progressive modes with equal shoreline elevation (noise to signal ratio NSR = 0.1). See Fig. 5 caption for further description.

wave fields. The deterministic synthetic matrices were generated from the discrete inverse form of Eq. (2) using beach slopes and sensor positions appropriate to each of the two study beaches. The test spectra discussed here (others have been examined) contained the first eight progressive modes traveling up and downcoast with equal *shoreline elevation amplitude* [a_n = 1, Eqs. (4), (5)] at all frequencies. Each edge wave mode was given a Gaussian shape in wavenumber space, with a half power wavenumber bandwidth of $2\pi(0.001)$ m^{-1}, which was a commonly observed estimated bandwidth of low mode edge waves at both beaches (section 6). Statistical fluctuations (after Brennan and Mallet, 1976) and uniform broad band noise were included in the synthetic spectra. Spectra were generated with ratios of total broad band noise to total edge wave energy ratios (hereafter NSR) of 0.1 and 0.9, and 40 and 400 degrees of freedom.

An example of estimator performance at f = 0.019 Hz is shown in Fig. 4. At this frequency and array location, the true energy spectrum is dominated by mode 0 (Fig. 8a). The higher modes appear in the true spectrum as a single low wavenumber peak because of their close proximity in wavenumber space; their half-power bandwidths overlap to create a smooth, single peak.

Synthetic True and IMLE longshore current k–f spectrum at the Santa Barbara array are shown in Fig. A1. IMLE performs best in the lower frequency range of 0.013 to 0.029 Hz where mode 0 edge waves dominate the true longshore velocity spectrum with approximately 84% of the energy. With 40 degrees of freedom and NSR = 0.1, the estimated variance in up- and downcoast propagating waves (in individual frequency bins) had standard deviations equal to about 20% of the true value. In contrast, with 400 degrees of freedom the standard deviation was less than 5%. Typical DOF in the field data are around 40, so apparent asymmetries in the direction of energy propagation in individual frequency bins may be associated with statistical fluctuations. To increase the stability of field

TABLE A1. True and IMLE half-power bandwidth (HPBW) and percentage of total power in mode 0 peaks (both HPBW and valley-to-valley) averaged over the 0.013–0.029 Hz band. DOF = 40 and noise to signal ratios of 0.1 and 0.9.

	HPBW (m^{-1})	Percent power within HPBW Upcoast		Percent power within Downcoast	
TRUE (NSR = 0.1)	0.0011	26.0	26.0	42.0	42.0
IMLE (NSR = 0.1)	0.0015	30.3	32.3	41.5	42.5
TRUE (NSR = 0.9)	0.0011	16.2	16.2	26.4	26.4
IMLE (NSR = 0.9)	0.0024	20.6	20.3	24.9	24.9

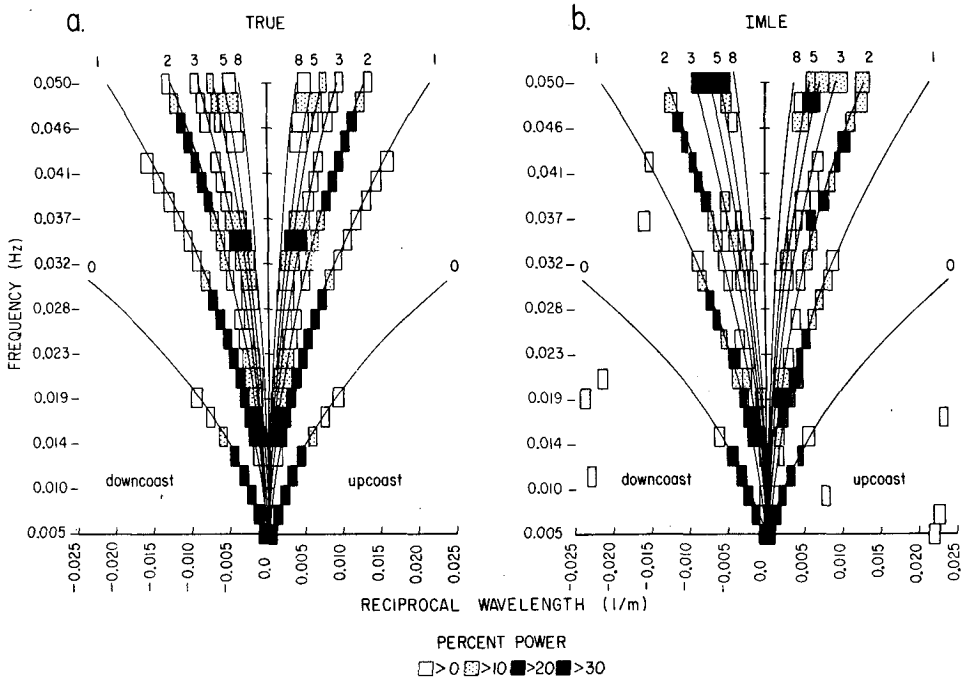

FIG. A2. The (a) true and (b) IMLE wavenumber-frequency spectra from a simulated longshore velocity signal at Torrey Pines (x = 66 m, β = 0.025). The velocity signal contains the same equal shoreline elevation edge wave field as Fig. A1 (NSR = 0.1, DOF = 40).

data estimates, the relative amounts of up and downcoast propagating energy were averaged over many frequency bins. Table A1 shows this procedure works well for synthetic data. The half-power bandwidth of peaks and the percentage of the total power contained within the peaks are also well estimated with a low signal to noise (Table A1). Increased noise degrades the estimates, particularly the half power bandwidth. The NSR of the field data is very roughly 0.1 (Figs. 4 and 6).

Averaged over the upper frequency band (0.036 to 0.05 Hz) of the true spectrum, mode 0 edge waves at the array have less than 2% of the longshore current variance. Mode 1 dominates with 55% of the variance with modes 2 and higher contributing 24% (Fig. A1a). This frequency band illustrates the estimators behavior when several peaks of near equal energy are close in wavenumber space. The estimated peak wavenumber locations are distorted and the half-power bandwidths are broadened. The true edge wave energy distribution is not as well estimated as in the lower frequency band.

Because of the differing beach slopes and offshore array locations, the mode 0 edge wave signal is detectable at a lower frequency at Torrey Pines (Fig. A2) than at Santa Barbara (Fig. A1). Additionally, mode 2 is apparent in the upper frequency band at Torrey Pines. The most important observation is that the array geometry at Torrey Pines does not grossly alter the behavior of the spectrum estimators from that at Santa Barbara; the wavenumber location and percent power of the peaks are also reasonably well estimated. The combination of a shallower beach slope (larger k for fixed frequency) and a longer array length at Torrey Pines does however allow resolution of mode 0 edge waves at lower frequencies. The lowest frequencies plotted (Figs. A1 and A2) are 0.005 and 0.009 Hz at Torrey Pines and Santa Barbara, respectively, and are the low frequency limits for the field data analysis.

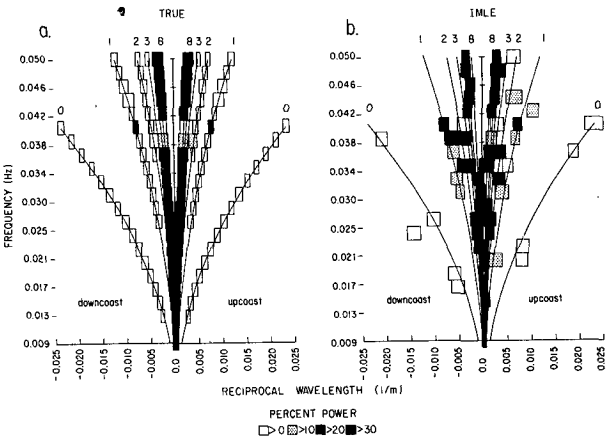

FIG. A3. The (a) true and (b) IMLE wavenumber-frequency spectra from a simulated cross-shore velocity signal at Santa Barbara (x = 26 m, β = 0.045). The velocity signal contains the same equal shoreline elevation edge wave field as Figs. A1 and A2 (NSR = 0.1, DOF = 40).

Unlike the simulated longshore current signal at the arrays, the simulated cross-shore current signal is strongly dominated by the high-mode edge waves (Figs. 8b, d), and as seen in the field data, the arrays (and estimators) do not consistently identify the low modes (Fig. A3).

REFERENCES

Ball, F. K., 1967: Edge waves in an ocean of finite depth. *Deep Sea Res.*, **14**, 79–88.

Bowen, A. J., and R. T. Guza, 1978: Edge waves and surf beat. *J. Geophys. Res.*, **83**, 1913–1920.

——, and D. L. Inman, 1969: Rip currents: 2. Laboratory and field observations. *J. Geophys. Res.*, **74**, 5479–5490.

——, and ——, 1971: Edge waves and crescentic bars. *J. Geophys. Res.*, **76**, 8662–8671.

Brennan, L. E., and J. D. Mallett, 1976: Efficient simulation of external noise incident on arrays. *IEEE Trans. Antenn. Propag.*, **24**, 740–741.

Davis, R. E., and L. Regier, 1977: Methods for estimating directional wave spectra from multielement arrays. *J. Mar. Res.*, **35**, 453–477.

Gable, C. G., (Ed), 1981: Report on data from the Nearshore Sediment Transport Study Experiment at Leadbetter Beach, Santa Barbara, California, January–February 1980, *IMR Ref. No. 80-5.*, University of California, Inst. Mar. Resour., La Jolla, CA, 314 pp.

Gallagher, B., 1971: Generation of surf beat by nonlinear wave interactions. *J. Fluid Mech.*, **49**, 1–20.

Guza, R. T., 1974: Comment on "Standing waves on beaches" by J. N. Suhayda. *J. Geophys. Res.*, **79**, 5671–5672.

——, and E. B. Thornton, 1985: Observations of surf beat. *J. Geophys. Res.*, **90**, 3161–3172.

Holman, R. A., 1981: Infragravity energy in the surf zone. *J. Geophys. Res.*, **86**, 6442–6450.

——, and A. J. Bowen, 1979: Edge waves on complex beach profiles. *J. Geophys. Res.*, **84**, 6339–6346.

——, D. A. Huntley and A. J. Bowen, 1978: Infragravity waves in storm conditions. *Proc. 16th Coastal Engineering Conf.*, 268–284.

Huntley, D. A., 1976: Long-period waves on natural beaches. *J. Geophys. Res.*, **81**, 6441–6449.

——, R. T. Guza and E. B. Thornton, 1981: Field observations of surf beat: 1. Progressive edge waves. *J. Geophys. Res.*, **86**, 6451–6466.

Longuet-Higgins, M. S., and R. W. Stewart, 1962: Radiation stress and mass transport in gravity waves, with application to "surf beats." *J. Fluid Mech.*, **13**, 481–504.

Munk, W., F. Snodgrass and F. Gilbert, 1964: Long waves on the continental shelf: An experiment to separate trapped and leaky modes. *J. Fluid Mech.*, **20**, 529–554.

Oltman-Shay, J., 1985: Infragravity edge wave observations on two California beaches. Ph.D. dissertation, Scripps Instit. of Oceanogr., University of California, San Diego, 111 pp.

——, and R. T. Guza, 1984: A data adaptive ocean wave directional-spectrum estimator for pitch and roll type measurements. *J. Phys. Oceanogr.* **14**(11), 1800–1810.

Pawka, S. S., 1982: Wave directional characteristics on a partially sheltered coast. Ph.D. dissertation, Scripps Instit. of Oceanogr., University of California, San Diego, pp. 246.

——, 1983: Island shadows in wave directional spectra. *J. Geophys. Res.*, **88**, 2579–2591.

Regier, L. A., and R. E. Davis, 1977: Observations of the power and directional spectrum of ocean surface waves. *J. Mar. Res.*, **35**, 433–452.

Snodgrass, F. E., W. H. Munk and G. R. Miller, 1962: Long-period waves over California's continental borderland. Part I. Background spectra. *J. Mar. Res.*, **20**, 3–30.

Suhayda, J. N., 1974: Standing waves on beaches. *J. Geophys. Res.*, **79**, 3065–3071.

Symonds, G., D. A. Huntley and A. J. Bowen, 1982: Two-dimensional surf beat: Longwave generation by a time-varying breakpoint. *J. Geophys. Res.*, **87**, 492–498.

Ursell, F., 1952: Edge waves on a sloping beach. *Proc. Roy. Soc.*, **A214**, 79–98.